Received XX Month, XXXX; revised XX Month, XXXX; accepted XX Month, XXXX; Date of publication XX Month, XXXX; date of current version 11 January, 2024.

Digital Object Identifier 10.1109/OJCOMS.2024.011100

Channel-Prediction-Driven Rate Control for LDPC Coding in a Fading FSO Channel with Delayed Feedback

SEMIRA GALIJASEVIC[1] *(Student Member, IEEE)*, JINGCHAO LUO [1] *(Student Member, IEEE)*, DARIUSH DIVSALAR [2] *(Life Fellow, IEEE)* AND RICHARD WESEL[1] *(Fellow, IEEE)*

[1]Department of Electrical and Computer Engineering, University of California, Los Angeles, CA USA
[2]Jet Propulsion Laboratory, California Institute of Technology, Pasadena, CA, 91109 USA

CORRESPONDING AUTHOR:Semira Galijasevic (e-mail: semiragali@g.ucla.edu).

This work was supported by CACI under award P000139095 and the National Science Foundation (NSF) under Grant CCF-1955660. Any opinions, findings, and conclusions or recommendations expressed in this material are those of the author(s) and do not necessarily reflect views of NSF. This work was carried out in part at the Jet Propulsion Laboratory, California Institute of Technology, under a contract with NASA.

ABSTRACT

Rate-adaptive coding enables reliable communication while efficiently utilizing the available channel mutual information in free-space optical (FSO) communication. While adaptive coding has been explored in numerous articles, the effect of feedback delay is often overlooked. To adapt the code rate to current channel conditions, the transmitter must sense the channel or rely on receiver feedback. FSO channel state information (CSI) cannot be reliably estimated at the transmitter because optical scintillation caused by atmospheric turbulence may differ for signals traveling in opposite directions. In real-world FSO systems, feedback from the receiver provides CSI. Even if the receiver sends accurate CSI, the channel conditions might change by the time the feedback reaches the transmitter and the new signal travels to the receiver. To mitigate throughput performance degradation caused by feedback delay, this paper applies linear and quadratic prediction to estimate future CSI and dynamically select the appropriate low-density parity-check (LDPC) code rate. Protograph-based Raptor-like (PBRL) LDPC codes supporting a wide range of rates are designed, facilitating convenient rate switching. When CSI is known without delay, dynamically selecting LDPC code rate appropriately maximizes throughput. This work explores how such prediction behaves as the feedback delay is increased from no delay to a delay equal to the coherence time of a fading channel. Optical channels with coherence times of $5\ ms$ and $10\ ms$ are explored, where $10\ ms$ channel is meant to model the optical channel of a Low Earth Orbit (LEO) satellite.

INDEX TERMS channel state information, free-space optical channel, LDPC codes, rate-adaptive coding

I. INTRODUCTION

A. Background

FREE-SPACE OPTICAL (FSO) communication [1] offers numerous benefits including high data rates, vast unlicensed free spectrum, high immunity to interference, highly secure links and easy installation [2]–[4]. FSO channels can be used for communications over distances of several kilometers as well as ultra-long distances including ground-to-satellite, satellite-to-satellite communications, and interplanetary communications [4].

FSO links are sensitive to channel fading caused by atmospheric turbulence, varying weather conditions, and changes in the distance between the transmitter and receiver. Because of this fading, hybrid communication systems are sometimes deployed where an RF link is used when the FSO link fails [5]–[8]. A novel coding paradigm called "Hybrid Channel Coding" that constructs non-uniform and rate-compatible low-density parity-check (LDPC) codes to achieve the combined channel capacity of parallel FSO and RF channels is introduced in [9].

Simulation analysis in [9] shows that Hybrid Channel Codes can increase the average throughput more than 33% compared to prior systems.

FSO fading has also been mitigated by adaptive parameter selection techniques such as those explored in [10]–[14]. The authors of [10] introduced a rate-adaptive transmission scheme employing intensity modulation and direct detection over FSO channels. The scheme uses repetition coding and variable silence periods to exploit the potential time-diversity order available in the fading channel.

Similarly, the study in [11] investigated punctured digital video broadcast satellite standard (DVB-S2) LDPC codes combined with channel interleavers to utilize time diversity. The combination of channel coding and bit interleaving in [11] improves performance in turbulence conditions.

In [12], three adaptive modulation schemes have been explored: (i) variable-rate variable-power adaptation, (ii) channel inversion, and (iii) truncated channel inversion schemes. CSI is estimated at the receiver and fed back to the transmitter through RF channel without considering feedback delay. The results show that channel inversion scheme gives similar performance compared to variable-rate variable-power scheme when turbulence is weak but suffers from significant performance degradation when turbulence is strong.

To mitigate FSO fading, a scheme to estimate the channel state information (CSI) at the receiver for Raptor and punctured LDPC code rate selection is proposed in [13]. The receiver sends estimated CSI through a feedback channel to the transmitter where the code rate is selected to accommodate estimated fading channel conditions. The proposed feedback scheme for both coding schemes is evaluated over a short transmission range such that feedback delay is not significant compared to the coherence time of the fading.

A rate-adaptive scheme using LDPC codes with optimized puncturing is compared to uncoded FSO system and coded FSO system using LDPC codes with random puncturing scheme in [14]. Results show that rate-adaptive systems perform well in realistic FSO systems over different weather conditions. For example, under rainy weather conditions uncoded FSO systems suffer from outages 87% of the time. In contrast, LDPC rate-adaptive systems can successfully utilize 75% to 80% of the signaling rate resulting in a significant increase in throughput. In [14], the rate is selected based on the CSI estimate at the receiver and sent back to the transmitter through an error-free feedback channel. However, in [14] the code rate selection does not consider how delay in the feedback channel can impact performance.

This paper investigates the effect of feedback delay on rate-adaptive FSO system with LDPC coding. Rate-adaptive LDPC codes provide significant coding gain [15] and efficient encoding and decoding with low hardware complexity [16], [17]. LDPC codes comprise the standard coding technique in Digital Video Broadcasting - Satellite, Second Generation (DVB-S2) [18] and are also utilized by Version 3.1.0 of the Optical Communications Terminal (OCT) Standard Developed by the Space Development Agency of the United States Space Force [19].

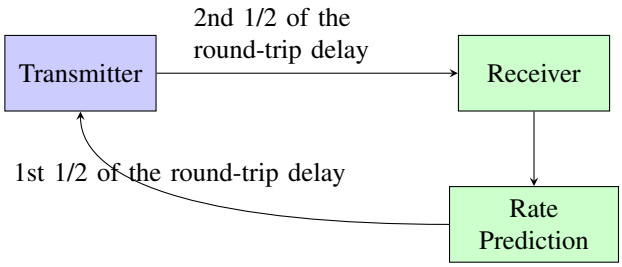

FIGURE 1. Simplified block diagram illustrating round-trip delay in using feedback for rate control. The first half of the round-trip delay is the duration from when the receiver sends back the predicted rate until the transmitter receives it. The second half of the round-trip delay is the duration for the signal encoded at the selected rate to travel from the transmitter to the receiver.

To minimize performance degradation caused by feedback delay, this paper uses predictive models to estimate fading channel conditions and dynamically select LDPC code rate. This achieves reliable communication while efficiently utilizing the available channel mutual information. The three predictive models explored are zero-order prediction, linear prediction, and quadratic prediction.

This work examines how these predictive models behave as the feedback delay is increased from no delay to a delay equal to the coherence time of the channel. Optical channels with coherence times of $5\ ms$ and $10\ ms$ are explored. Protograph-based Raptor-like (PBRL) LDPC codes with rates $8/9$, $8/10$, ..., $8/80$ are designed using reciprocal channel approximation (RCA) [20] allowing convenient rate switching.

The feedback delay is the round-trip delay, i.e., the time between when the receiver makes the rate prediction and when the LDPC codeword at the selected rate arrives at the receiver experiencing a fade. A simple block diagram in Fig. 1 illustrates the round-trip feedback delay. The first half of the round-trip delay is the time it takes for the rate selection signal to travel back to the transmitter after the receiver predicts the rate. The second half of the round-trip delay is the signal propagation time from the transmitter to the receiver. Thus, the receiver experiences the fade one round-trip time after sending the prediction.

Note that there is an additional small time at the transmitter to compute the codeword after receiving the prediction. However, this could be very small or even negligible since the transmission can start even slightly before the rate guidance arrives since the rate determines the total number of symbols and the transmitter will always send at least the number of symbols for the highest rate. An additional time also occurs for the receiver to compute the prediction, which is negligible compared to the total feedback delay.

The optical channel with a coherence time of $10\ ms$ is meant to model the optical channel of a Low Earth Orbit

TABLE 1. Orbital distances and corresponding round-trip feedback delays of common LEO systems.

LEO system	Orbital Distance (km)	Round-Trip Feedback Delay (ms)
Starlink (SpaceX)	$340-570$	$2.2-3.8$
International Space Station (ISS)	$408-420$	$2.7-2.8$
Hubble Space Telescope	535	3.6
TROPICS (NASA)	550	3.6
Planet Labs' Dove Satellites	$400-500$	$2.7-3.4$
Kuiper (Amazon)	$590-630$	$4.0-4.2$
Landsat (NASA/USGS)	705	4.7
Sentinel (ESA)	$700-786$	$4.6-5.2$
Iridium Next	780	5.2
NOAA JPSS	824	5.5
OneWeb	1200	8.0
Globalstar	1400	9.3

(LEO) satellite. A typical LEO system usually operates at altitudes ranging from around 160 kilometers (km) (99 miles) to $2,000$ km ($1,240$ miles). The distance between an Earth station and a LEO satellite corresponding to the specific round-trip feedback delay time is calculated as $c \times t_d/2$, where $c = 3 \times 10^8 m/s$ is speed of light and t_d is round-trip feedback delay time. The round-trip delay times of $2-10$ ms correspond to distances of 300 to 1500 km.

Table 1 provides the orbital distances of various common LEO systems. The International Space Station (ISS), for example, has an orbital distance of $408-420$ km while SpaceX's Starlink satellites orbit Earth at a distance of about $340-570$ km above sea level. The project Kuiper satellites will have an orbit between 590 and 630 kilometers. The Iridium satellites orbit at about 780 km. Earth observation satellites such as Landsat satellites operate around 705 km.

B. Contributions

The following contributions are from our previously published conference paper [21].

- Design of 72 PBRL LDPC codes supporting a wide range of rates from $8/9$ to $8/80$. The rates are designed using RCA [20] to minimize the decoding threshold.
- The analysis shows when CSI is known with no delay, dynamically selecting LDPC code rate based on the CSI maximizes throughput. Such throughput is referred as the zero-delay throughput in this paper.
- Zero-order, linear, and quadratic prediction models are explored to estimate fading channel CSI and dynamically select the LDPC code rate. The optical channel coherence time used for analysis is 10 ms and round-trip feedback delay times explored range from no delay to delay equal to 4 ms.

This paper extends [21] by:

- Providing a detailed analysis of the channel model and the simulation method used to generate realizations of temporal fading.
- Incorporating estimation of CSI at the receiver to make prediction models more applicable for real-world implementation.
- Studying optical channels with shorter coherence times such as 5 ms in addition to the explored coherence time of 10 ms.
- Improving the linear and quadratic prediction models by optimizing the number of fading channel gain samples used to predict future channel conditions and appropriately select LDPC code rate.
- Extending round-trip feedback delay times from no delay to delay equal to the coherence time of optical channel.
- Analyzing computational complexity of the proposed prediction models.
- Exploring how round-trip delay affects common LEO systems in terms of their orbital distance.

C. Organization

The rest of the paper proceeds as follows. Sec. II introduces the system architecture and FSO channel model. Sec. III presents a estimates FER for LDPC codes in the modeled channel using the normal approximation. Sec. IV describes LDPC codes designed for a wide range of rates. Sec. V describes three prediction models and presents throughput results achieved by using these predictive models to select the LDPC code rate. Sec. VI concludes this paper.

II. System Architecture and Fading Channel Model

A. System Architecture

Fig. 2 describes the high-level system architecture. The receiver estimates the fading channel and uses it to decode the current codeword. The receiver also uses the estimated channel gains to predict the future channel gain and corresponding LDPC code rate at a specified future time, which is based on the delay required to transmit the code rate to the transmitter. The receiver selects the future LDPC code rate such that selected code rate achieves frame error rate (FER) lower than 10^{-6} for predicted channel gain value.

Fig. 3 shows FER curves for a subset of the designed LDPC codes as a function of fading channel gain. None of our LDPC code rates suffer from an error floor above 10^{-6}. The highest code rate $(8/9)$ is the rightmost curve.

The channel gain values corresponding to FERs 10^{-6} in Fig. 3 for each code rate are referred as "crossing points" and shown in Table 2 in the LDPC Simulation Crossing Point column. The crossing points in Table 2 are calculated by subtracting baseline average power on detector (P_{ave}) of

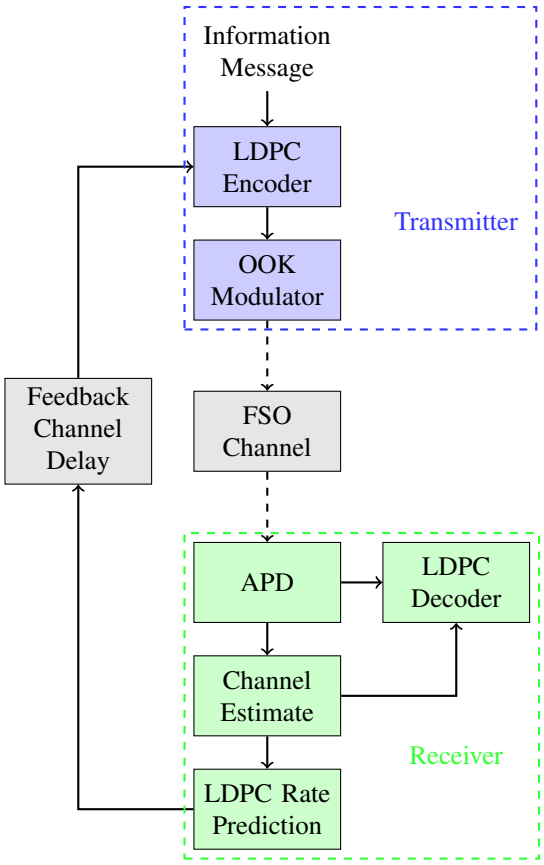

FIGURE 2. **High-level system block diagram. The fading channel gain is estimated at the receiver and used to decode the current codeword as well as to predict the future channel gain and corresponding LDPC code rate based on the round-trip delay. The receiver selects the future LDPC code rate such that selected code rate achieves frame error rate (FER) lower than 10^{-6} for predicted channel gain value. The time required for the transmitter to receive a predicted codeword via the feedback channel is equal to half of the round-trip delay.**

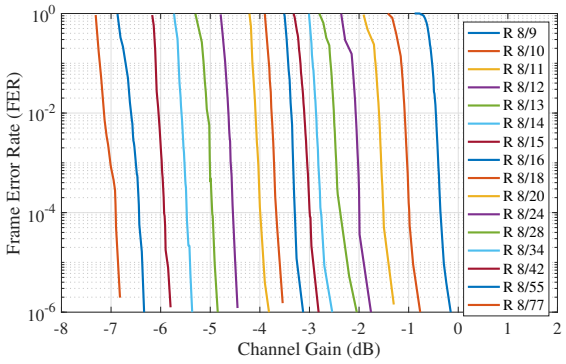

FIGURE 3. **Frame Error Rate (FER) Vs. Channel Gain for LDPC code rates $8/9$ to $8/77$ in descending order from right to left.**

$-48.1\ dBm$ from P_{ave} for which LDPC code rate achieves FER of 10^{-6}.

The selected LDPC code rate is sent back to the transmitter through an error-free feedback channel with round-trip feedback delay time t_d. The information message is generated at the transmitter side and encoded with LDPC encoder with rate equal to the code rate received via the delayed feedback channel.

TABLE 2. **LDPC codes with channel gain crossing points. Each code rate achieves FER of 10^{-6} for corresponding crossing point.**

Code Rate	LDPC Simulation Crossing Point [dB]	Normal Approx. Crossing Point [dB]
8/9	-0.1522	-0.5550
8/10	-0.7672	-1.4700
8/11	-1.2802	-2.0800
8/12	-1.7596	-2.5400
8/13	-2.0459	-2.9200
8/14	-2.5409	-3.2500
8/15	-2.8154	-3.5300
8/16	-3.1276	-3.7800
8/18	-3.5267	-4.2100
8/20	-3.8154	-4.5000
8/24	-4.4457	-5.1600
8/28	-4.8492	-5.6300
8/34	-5.3644	-6.1900
8/42	-5.7939	-6.7700
8/55	-6.3336	-7.4800
8/77	-6.8036	-8.3200

B. Fading Channel Model

The channel model (given the fade power ρ) is an asymmetric Gaussian model based on experimentally measured gains in communications performance of a laboratory-based, free-space optical communications system using an avalanche photodiode detector (APD) at the receiver for signal detection [22]. Following [8] and [23], to compute realizations of temporal fading a sequence of independent and identically distributed (i.i.d.) Gaussian random numbers z_i is filtered by a low-pass finite impulse response (FIR) filter with the frequency response described in (1).

$$H(f) = \sqrt{{\sigma_L}^2 \tau_0 \sqrt{\pi}} \exp\left(-\frac{1}{2}(\pi \tau_0 f)^2\right). \tag{1}$$

The filtered z_i values produce a band-limited discrete sequence x_i of correlated Gaussian random variables with variance $\sigma_L^2 = \ln({\sigma_T}^2 + 1)$, where σ_T^2 is the Power Scintillation Index (PSI) characterizing the depth of scintillations.

Generated samples x_i are transformed to obtain the desired log-normal distribution of correlated fading realizations ρ_{T_i} as follows:

$$\rho_{T_i} = \exp\left(x_i - {\sigma_L}^2/2\right). \tag{2}$$

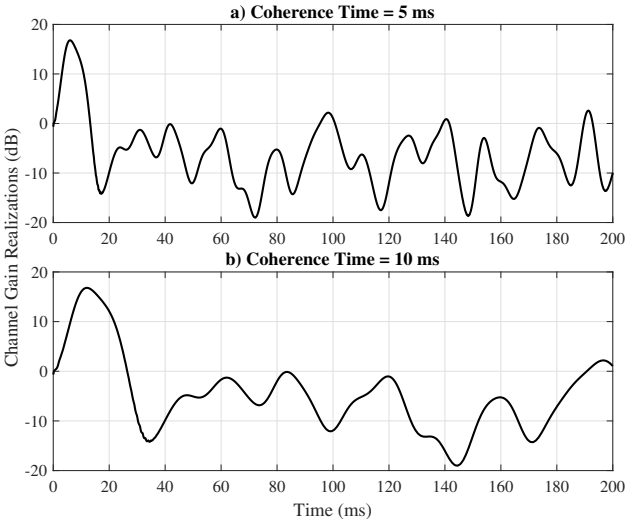

FIGURE 4. Fading channel gain realizations ρ_{T_i} in dB as a function of time for turbulence coherence time of a) $5\ ms$ and b) $10\ ms$.

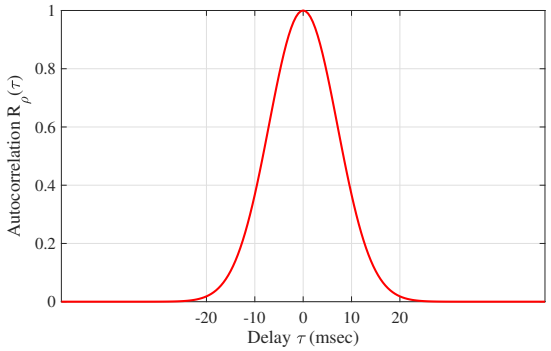

FIGURE 5. Autocorrelation function $R_\rho(\tau)$ for turbulence coherence time of $\tau_0 = 10\ ms$.

Fig. 4 depicts fading channel realizations ρ_{T_i} in dB for turbulence coherence times of 5 ms and 10 ms.

The autocorrelation function of the log amplitude of scintillation is approximated as

$$R_\rho(\tau) = (\ln(\sigma_T^2 + 1))^2 \exp[-(\tau/\tau_o)^2], \tag{3}$$

where τ_0 denotes turbulence coherence time [22]. Turbulence coherence time represents a time interval during which the change in fading characteristics of the channel is very small.

Fig. 5 shows autocorrelation function for turbulence coherence time of 10 ms as a function of delay τ. As the delay increases, the most recent observed fade and the predicted fade are less and less correlated, and becoming completely uncorrelated when delay becomes longer than two times the coherence time. The less correlated the two fades are, the harder it is to predict the future fade.

The modulation scheme used is On-Off keying (OOK) such that each OOK slot contains either the signal (bit 1) or background noise (bit 0). Bit 1 is modulated to μ_1 and bit 0 is modulated to μ_0, where μ_1 is the signal current when the signal is ON and μ_0 is signal current when the signal is off. Additive white Gaussian noise (AWGN) is added to the signal so that observations for both signal (ON) for bit 1 and signal (OFF) for bit 0 are modeled using Gaussian distributions $\mathcal{N} \sim (\mu_1, \sigma_1^2)$ and $\mathcal{N} \sim (\mu_0, \sigma_0^2)$. Here, σ_1 and σ_0 denote total noise when the signal is on and off, respectively. Thus, the log-likelihood ratio (LLR) used by LDPC decoder is given by:

$$LLR = \frac{1}{2} \ln \frac{\sigma_0^2}{\sigma_1^2} + \frac{(y-\mu_0)^2}{2\sigma_0^2} - \frac{(y-\mu_1)^2}{2\sigma_1^2}. \tag{4}$$

Equations (5)–(12) describe the calculations of μ_1, σ_1, μ_0 and σ_0. The meanings and values of the variables and constants used in the equations are given in Table 3. Note that F is the APD excess noise factor, and $\rho(t)$ is the fading

TABLE 3. Constants and variables used to calculate signal current μ_1 and total noise σ_1 when signal is ON, and signal current μ_0 and total noise σ_0 when signal is OFF.

Symbol	Quantity	Value	Unit
q	electron charge	1.6×10^{-19}	C
G	Avalanche Photodiode gain APD	15	
$\mathcal{R}$	responsivity	0.9	A/W
B	electronic filter bandwidth	1250	MHz
k	impact coefficient	0.2	
I_{dark}	dark current	2.1×10^{-8}	A
D_{TIA}	Transimpedance Amplifier (TIA) input noise current density	2×10^{-12}	$\frac{A}{\sqrt{Hz}}$
P_{ave}	average power on detector	-48.1	dBm
r_{ext}	extinction ratio	11	dB
P_1	power on detector when bit 1 is sent	$P_{\text{ave}} + \frac{r_{ext}}{2}$	dBm
P_0	power on detector when bit 0 is sent	$P_{\text{ave}} - \frac{r_{ext}}{2}$	dBm
p_1	power on detector when bit 1 is sent	$10^{P_1/10}$	mW
p_0	power on detector when bit 0 is sent	$10^{P_0/10}$	mW

realization at time t.

$$\mu_1(t) = \frac{1}{2} \times \mathcal{R} \times G \times \rho(t) \times p_1 = \rho(t)\mu_1^* \quad (5)$$

$$\mu_0(t) = \frac{1}{2} \times \mathcal{R} \times G \times \rho(t) \times p_0 = \rho(t)\mu_0^* \quad (6)$$

$$F = k \times G + (1-k) \times \left(2 - \frac{1}{G}\right) \quad (7)$$

$$S_1(t) = (2 \times q \times \mu_1(t) \times G \times F)^{\frac{1}{2}} \quad (8)$$

$$S_0(t) = (2 \times q \times \mu_0(t) \times G \times F)^{\frac{1}{2}} \quad (9)$$

$$M = (2 \times q \times F \times G^2 \times I_{dark})^{\frac{1}{2}} \quad (10)$$

$$\sigma_1(t) = \left[B \times ((S_1(t))^2 + M^2 + D_{TIA}^2)\right]^{\frac{1}{2}} \quad (11)$$

$$\sigma_0(t) = \left[B \times ((S_0(t))^2 + M^2 + D_{TIA}^2)\right]^{\frac{1}{2}} \quad (12)$$

The electronic filter bandwidth B value of 1250 MHz is used for simulation purposes, but it can be higher in practice. Note that for the baud rate of 2.5 Giga symbols per second used in this paper, the time occupancy of each codeword ranges from 3.6864 microseconds (μs) for the highest code rate (8/9) to 31.539 μs for the lowest code rate (8/77), which is relatively small compared to the turbulence coherence times of 5 ms and 10 ms. The fading model generates one fade value for every 1024 bits, which means that different sections of a codeword will experience a different fade. However, since the turbulence coherence time is much longer than the time occupancy of a codeword, these differences are negligible.

III. Normal Approximation of Frame Error Rate

For FSO On-Off Keying (OOK) with equally likely transmission of bits 1 and 0, consider the following channel model when bit 1 (On) or bit 0 (Off) is transmitted:

$$y = \mu_i + \sigma_i n, \quad i = 0 \text{ or } 1 \ , \quad (13)$$

where n is a zero mean, unit variance normal (Gaussian) random variable. The mean μ_i already includes the fading $\rho(t)$ as described in Sec. B. The received value y is a Gaussian random variable with probability density function $f_i(y)$ which is normal distributed $\mathcal{N}(\mu_i, \sigma_i^2)$.

When bit 1 is transmitted the channel information density is

$$i_1(y) = 1 - \log_2\left(1 + \frac{\sigma_1}{\sigma_0} e^{-\frac{1}{2\sigma_0^2}(y-\mu_0)^2 + \frac{1}{2\sigma_1^2}(y-\mu_1)^2}\right) \quad (14)$$

and its nth moment after change of variable is

$$m_n(i_1) = \int_{-\infty}^{\infty} f_1(y) i_1^n(y) dy = \int_{-\infty}^{\infty} \frac{1}{\sqrt{2\pi}} e^{-\frac{z^2}{2}} i_1^n(z) dz \ ,$$

where

$$i_1(z) = 1 - \log_2\left(1 + \frac{\sigma_1}{\sigma_0} e^{-\frac{1}{2\sigma_0^2}(\sigma_1 z + \mu_1 - \mu_0)^2 + \frac{1}{2}z^2}\right).$$

When bit 0 is transmitted the channel information density is

$$i_0(y) = 1 - \log_2\left(1 + \frac{\sigma_0}{\sigma_1} e^{-\frac{1}{2\sigma_1^2}(y-\mu_1)^2 + \frac{1}{2\sigma_0^2}(y-\mu_0)^2}\right) \quad (15)$$

and its nth moment after change of variable is

$$m_n(i_0) = \int_{-\infty}^{\infty} f_0(y) i_0^n(y) dy = \int_{-\infty}^{\infty} \frac{1}{\sqrt{2\pi}} e^{-\frac{z^2}{2}} i_0^n(z) dz \ ,$$

where

$$i_0(z) = 1 - \log_2\left(1 + \frac{\sigma_0}{\sigma_1} e^{-\frac{1}{2\sigma_1^2}(\sigma_0 z + \mu_0 - \mu_1)^2 + \frac{1}{2}z^2}\right).$$

The average of channel information density with equally likely channel inputs of zero or one is

$$I = \frac{1}{2}[m_1(i_1) + m_1(i_0)] \quad (16)$$

and the channel dispersion with equally likely channel inputs of zero or one is

$$V = \frac{1}{2}[m_2(i_1) + m_2(i_0)] - I^2. \quad (17)$$

Both $I(P_{ave})$ and $V(P_{ave})$ are functions of the average received power P_{ave} at APD.

Using the Normal Approximation (NA) by Polyanskiy et al. [24], the maximal achievable rate can be approximated by

$$R^*(n, FER) = I - \sqrt{\frac{V}{n}} Q^{-1}(FER) + O(\frac{\log_2 n}{n}), \quad (18)$$

where $Q^{-1}(.)$ denotes inverse of the Gaussian Q-function which is

$$Q(x) = \int_x^{\infty} \frac{1}{\sqrt{2\pi}} e^{-\frac{1}{2}y^2} dy. \quad (19)$$

Then the normal approximation on frame error rate FER_{NA} can be calculated as

$$\text{FER}_{\text{NA}}(P_{ave}) = Q\left(\frac{I(P_{ave}) - R + \log_2(n)/2n}{\sqrt{V(P_{ave})/n}}\right) \ , \quad (20)$$

where R represent the code rate, $n = k/R$ is codeword block length, k is the message block length, and $O(\frac{\log_2 n}{n}) \approx \log_2(n)/2n$. However, for $k = 8192$ the same FERs have been obtained for all code rates by ignoring the $O(.)$ term.

As an example, consider a laser with extinction ratio of 11 dB, and an APD detector, such that observations can be expressed as, $\mu_1 = \alpha_1 P_{ave}$, $\mu_0 = \alpha_0 P_{ave}$, $\sigma_1^2 = \beta_1 P_{ave} + \gamma_1$, and $\sigma_0^2 = \beta_0 P_{ave} + \gamma_0$, where $\alpha_1 = 47.9$, $\alpha_0 = 3.8$, $\beta_1 = 1.3\times10^{-6}$, $\beta_0 = 1\times10^{-7}$ and $\gamma_1 = \gamma_0 = 1.36\times10^{-14}$. In this paper block fading is considered where the fade power ρ is constant over duration of codeword. This assumption is valid when the coherence time of fading is larger than duration of codeword. The fading power is normalized such that $E\{\rho\} = 1$.

In the fading channel model, P_{ave} is then replaced with ρP_{ave}. For atmospheric fading the Power Scintillation Index $PSI = {\sigma_T}^2 = 10$ is assumed.

The FERs using normal approximation for rates 8/9 to 8/77 are plotted in Fig. 6. The crossing points representing fading channel gain values at which FERs for normal approximation are 10^{-6} are listed in Table 2. For LDPC simulations, crossing points are computed based on the reference point average P_{ave} of -48.1 dBm.

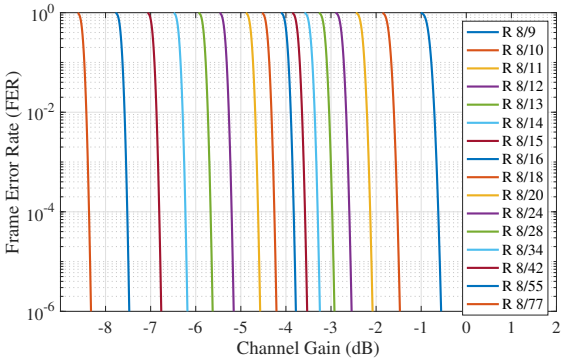

FIGURE 6. **Frame Error Rate (FER) vs Channel Gain using Normal Approximation (NA).**

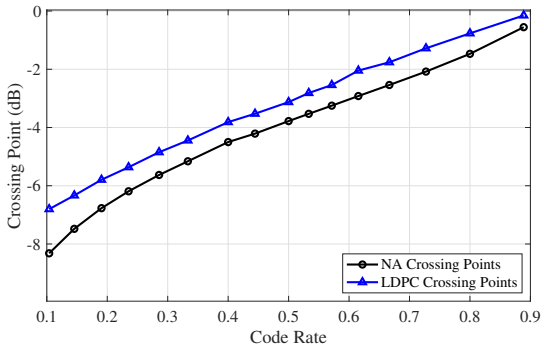

FIGURE 7. **The crossing points in Table 2 are compared with crossing points using normal approximation (NA).**

Fig. 7 presents a comparison between the crossing points derived from LDPC simulations and those obtained through the normal approximation. The gap between the simulated LDPC code FER crossing points and those resulting from the normal approximation of random code performance ranges from $0.4\ dB$ to $1.5\ dB$. The close proximity of the normal approximation to the actual LDPC code performance adds confidence that the LDPC codes are well-designed across the entire range of rates.

One way to see how adaptively adjusting the rate can improve performance for slow fading is to compute the $\text{FER}_{\text{fixed}}$ that a fixed-rate system would provide. To compute the theoretical performance of a fixed-rate scheme in slow fading without feedback, we integrate the product of the density $f(\rho)$ of ρ from [23] and the FER from (20) (denote that by $F(P_{ave})$) with P_{ave} replaced with ρP_{ave} for a fixed-rate random code, as shown below:

$$\text{FER}_{\text{fixed}} = \int_{\rho=0}^{\infty} \text{FER}_{\text{NA}}(\rho P_{ave}) f(\rho) d\rho \ , \qquad (21)$$

assuming that the pdf $f(\rho)$ of fade power ρ is normalized such that $E\{\rho\} = 1$. Such a computation reveals that the FER performance for the fixed-rate scheme incurs a huge performance loss.

IV. Low-Rate Protograph-based LDPC Codes Design

This paper uses the Protograph-Based Raptor-Like (PBRL) [20] approach to design LDPC codes with information blocklength $k = 8192$ and parity check matrix $\mathbf{H}$ described by (22) for wide range of rates:

$$\mathbf{H} = \begin{bmatrix} \mathbf{H}_{\text{HRC}} & \mathbf{0} \\ \mathbf{H}_{\text{IRC}} & \mathbf{I} \end{bmatrix}. \qquad (22)$$

Let n_1 represent the number of variable nodes in $\mathbf{H_{HRC}}$, of which n_p are punctured to improve the iterative decoding threshold. Let m_1 number of rows in $\mathbf{H_{IRC}}$ matrix. In equation (22) submatrix $\mathbf{H}_{\text{HRC}} \in \mathbb{F}_2^{(n_1-k)\times n_1}$ represents a highest-rate code (HRC) and submatrix $\mathbf{H}_{\text{IRC}} \in \mathbb{F}_2^{m_1 \times n_1}$ represents an incremental redundancy code (IRC). PBRL LDPC code supports rates from $\frac{k}{n_1-n_p}$ to $\frac{k}{n_1+m_1-n_p}$. The rate is selected by deciding how many of the degree-1 variable nodes associated with identity matrix in (22) should be punctured. This work designs the $\mathbf{H}_{\text{IRC}}$ to support the lowest code rate of $1/10$. Thus, $m_1 = 72704$ and $n_1 = 9216$.

The parity check matrix $\mathbf{H}_{\text{HRC}}$ for the highest rate code is obtained by lifting a proto-matrix. The proto-matrix $\mathbf{H}_{\text{HRC-proto}}$ in (23) is adopted from [8].

$$\mathbf{H}_{\text{HRC-proto}} = [\ 4 \quad 4 \quad 4 \quad 4 \quad 4 \quad 3 \quad 3 \quad 3 \quad 3\ ] \qquad (23)$$

Unlike LDPC codes that start with a designed lowest rate code and increase the rate by randomly puncturing variable nodes hoping to not degrade performance, PBRL design starts with a well-designed highest-rate code and obtains lower-rate codes by carefully selecting the rows of $\mathbf{H}_{\text{IRC}}$.

The design of $\mathbf{H}_{\text{IRC}}$ is completed in two steps. In the first step, the proto-matrix $\mathbf{H}_{\text{IRC}}$ [25] is designed line by line in a greedy fashion by minimizing decoding threshold of newly constructed protograph matrix computed using the reciprocal channel approximation (RCA) algorithm [20]. The RCA is a fast and accurate approximation to the density evolution algorithm with deviation in accuracy of less than $0.01\ dB$. The decoding threshold of a protograph matrix refers to the minimum channel noise that supports reliable iterative decoding of LDPC codes with infinite code length built from the protograph. The fully designed protograph matrix of $\mathbf{H}$ for rate $1/10$ consists of 72 rows (check nodes) and 80 columns (variable nodes).

In the second step, the designed protograph matrix for lowest code rate of $1/10$ is lifted using approximate-cycle extrinsic-message-degree (ACE) progressive-edge-growth (PEG) algorithm [26] to replace each element in protograph matrix with circulant matrices and obtain parity check matrix $\mathbf{H}$ with longer block-length. The ACE-PEG algorithm with parameters of $d_{ACE} = 6$ and $\eta = 7$ are selected to ensure that all the cycles in the lifted parity check matrix whose length is 12 or less have ACE values of at least 7.

The lifting process also consists of two steps. In the first step, lifting number is 4 to remove parallel edges in protograph matrix. In the second step, lifting number is 256 which gives a parity check matrix with information

blocklength of 8192 bits. Fig. 3 shows FER as a function of fading channel gain for a subset of the designed LDPC code rates. Fig. 7 compares performance between designed LDPC codes and the normal approximation and random coding for FER of 10^{-6}.

V. LDPC Rate Selection To Maximize Throughput

This section presents different predictive models for selecting LDPC code rate based on the knowledge of channel gain and feedback time delays. The fading channel gains are estimated at the receiver and used to predict a future channel gain considering the round-trip delay required to transmit the feedback signal from the receiver back to the transmitter and new signal from the transmitter to the receiver. The receiver uses predicted channel gain values to select LDPC code rate that achieves FER lower than 10^{-6} for predicted channel gain. For the purpose of analysis, out of 72 designed code rates a subset of 16 code rates with approximate differences of 0.5 dB at crossing points at FER of 10^{-6} is selected. The channel gain crossing points for which each LDPC code rate decodes a codeword with FER of 10^{-6} are given in Table 2.

A. Instantaneous Channel State Information

As a baseline for comparison, we consider the case where the feedback delay is zero and current channel state is known. The LDPC code rate is selected to maximize throughput, i.e. the code rate selected is the highest code rate that achieves FER below 10^{-6} for the current known channel state. Actual channel gain data is represented with black curve in Fig. 4 for coherence times of 5 and 10 ms. Throughput achieved when the transmitter knows the CSI with no delay is referred as zero-delay throughput and it is used as a reference to evaluate the performance of prediction models when feedback delay is not zero.

Fig. 8 shows throughput as a function of time for optical channel with coherence time of 10 ms for a) rate-adaptive system when CSI is known at the transmitter with no delay, referred as zero-delay throughput, b) when single LDPC code rate $8/9$ is used, and c) when single LDPC code rate $1/2$ is used. The simulations, performed over 100 ms of data, indicate that throughput achieved when using single LDPC code rate is approximately 55.9% and 60.3% of zero-delay throughput for rates $8/9$ and $1/2$ respectively. Note that the optical channel realizations used for simulations consist of 30% of very good turbulence conditions boosting the performance of both $8/9$ and $1/2$ rates. As turbulence conditions become worse, the performance of using a fixed single rate drastically decreases, which is evident between 30 ms and 55 ms in Fig. 8 where both rates suffer from constant failure, making the throughput zero fo a significant fraction of the simulated time segment.

B. Delayed Channel State Information

Now we consider the practical scenario in which the feedback delay is not zero.

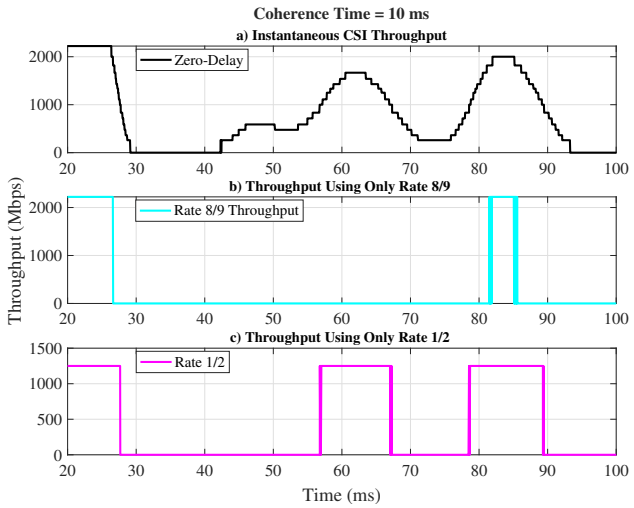

FIGURE 8. Throughput as a function of time for optical channel with coherence time of $10\ ms$. a) Throughput achieved using rate-adaptive LDPC coding when channel state information (CSI) is known. b) Throughput achieved when using LDPC code rate $8/9$ only. c) Throughput achieved when using LDPC code rate $1/2$ only.

1) CSI Estimation

Based on practical experience of the optical fading channel, our fading model assumes that fading is constant over 1024 OOK symbols. Even between groups of 1024 OOK symbols the fading changes very slowly. Because of this slow change in the fading, estimation of the fading at the receiver is not the key issue, the ability to predict future fading based on the knowledge of the current fading is the critical issue.

A simple fading channel gain estimation $\hat{\rho}(t)$ at the receiver is performed as follows. From equations (5) and (6) $\mu_1^* = \frac{1}{2} \times R \times G \times p_1$ and $\mu_0^* = \frac{1}{2} \times R \times G \times p_0$. Then $\mu_1(t) = \mu_1^* \times \hat{\rho}(t)$ and $\mu_0(t) = \mu_0^* \times \hat{\rho}(t)$. For a single value of $\hat{\rho}(t)$ we see 1024 observations of $\mu_1(t)$ and $\mu_0(t)$. In our estimation model we assume that out of 1024 bits there is equal possibility of getting bit 1 or bit 0, i.e. we generate 1024 Bernoulli distributed zeros and ones[1]. The receiver sees 1024 different observations of noisy signal $y(t) = \mu_i(t) + Z\sigma_i$, where $i \in \{0, 1\}$ and Z is Gaussian random variable with zero mean and unit variance. Then estimated $\hat{\rho}(t)$ is given by

$$\hat{\rho}(t) = \frac{\frac{1}{512}\sum_{j=1}^{1024} y_j(t)}{\mu_1^* + \mu_0^*}. \tag{24}$$

To improve the estimation of the noisier channels, once $\hat{\rho}(t)$ is obtained by (24) we average 9 adjacent measurements

[1]The generation of received noisy sequences of 1024 using Bernoulli distributed zeros and ones can be justified since in optical transmitter and specifically in the CCSDS optical standard usually a Pseudo-Randomizer is used at transmitter (see [27]). In addition, in the optical standard, Gold code sequences are used for frame synchronization (frame synch marker) with almost balanced zeros and ones with a difference of 1 between the two counts, which can also be used for CSI estimation provided that the coherence time is longer than the duration of synch marker and a codeword.

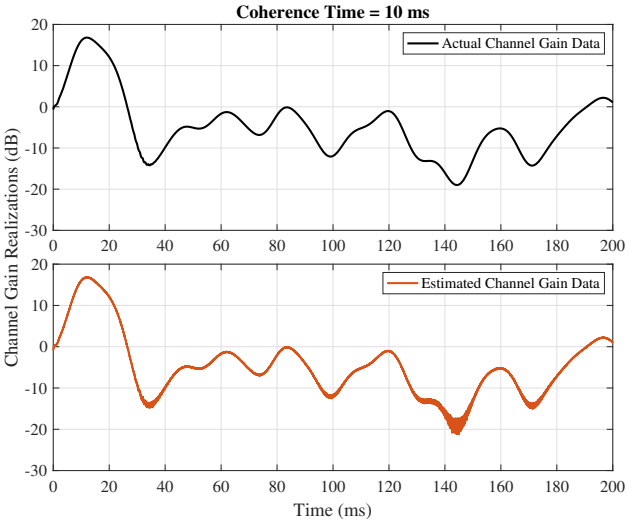

FIGURE 9. Comparison of actual and estimated fading channel gain data for coherence time of $10\ ms$.

and use that value for $\hat{\rho}(t)$. Note that 9 channel gain samples, each corresponding to 1024 bits, represent the duration of the codeword with the highest code rate of $8/9$.

Fig. 9 shows actual fading channel gain data generated in MATLAB using fading channel model in Sec. B and estimated fading channel gain data at the receiver given by (24). When the channel is relatively good (e.g. above $-10\ dB$), the received signal is less affected by noise, making the channel estimation more reliable and closer to the actual channel gain values resulting in low estimation error. When the channel is poor (e.g. below $-10\ dB$), the received signal is heavily corrupted by noise. This leads to higher uncertainty in the estimation process, causing the estimated fading channel gains to deviate significantly from the actual values and appear noisy which can be observed near $35\ ms$, $140\ ms$ and $170\ ms$ in Fig. 9.

2) Zero-Order Prediction

The zero-order prediction model predicts fading channel gain value in the future to be the same as the current channel estimate at the receiver. Let fading channel gain value estimated at the receiver at time t_k be $\hat{\rho}_k$ in dB and let t_d denote the feedback channel delay time. The predicted channel gain value $\tilde{\rho}_{k+d}$ at time $(t_k + t_d)$ is the same as estimated value $\hat{\rho}_k$.

3) Linear Prediction

Let $\hat{\boldsymbol{\rho}} = [\hat{\rho}_1, \hat{\rho}_2, ..., \hat{\rho}_n]$, $\hat{\rho}_i \in \mathbb{R}$ represent fading channel gain values estimated by the receiver. Let $\boldsymbol{t} = [t_1, t_2, ..., t_n]$, $t_i \in \mathbb{R}$ represent time instances that correspond to the estimated fading channel gain values in $\hat{\boldsymbol{\rho}}$. Note that $\hat{\rho}_n$ corresponds to the current time instance t_n, and all other samples in $\hat{\boldsymbol{\rho}}$ are past samples estimated at the receiver. The receiver only has knowledge of the past fading channel gain data measured at the receiver. In order to make a prediction of channel gain in the future, the estimated n samples is used to fit a polynomial of a form:

$$p(t) = x_1 + x_2\ t + ... + x_{m+1}t^m. \tag{25}$$

For each polynomial coefficient x a vector of errors $\boldsymbol{e} = [p(t_1) - \hat{\rho}_1, p(t_2) - \hat{\rho}_2, ..., p(t_n) - \hat{\rho}_n]$ is formed. As described in [28], to find a polynomial that minimizes the norm of the error vector $\boldsymbol{e}$ following norm approximation problem is solved:

$$\min_{\boldsymbol{x}} ||\boldsymbol{e}|| = ||\boldsymbol{A}\boldsymbol{x} - \hat{\boldsymbol{\rho}}||\ , \tag{26}$$

where $A_{ij} = t_i^{j-1}$, $i = 1, 2, ..., n$, $j = 1, 2, ..., (m+1)$. MATLAB function *polyfit* is used to solve problem in (26) to obtain polynomial coefficients $\boldsymbol{x}$. Once the polynomial model is fitted, its coefficients are used to predict future fading channel gain $\tilde{\rho}_{t_k}$ at some time instance t_k by plugging t_k into (25). The coding rate is predicted based on this predicted fading channel gain value. In the simulations when the codeword sent at this rate arrives at the receiver it will experience fade coming from the actual fading channel data which receiver never saw before. Note that the polynomial coefficients change for every prediction as the receiver keeps retraining the model in an "online" manner based on the new data it receives. Since the receiver does not have knowledge of the future true data, there is no testing or validation data. The only way to know if the prediction was accurate is by observing if the codeword that was sent at the predicted rate was successfully decoded.

For linear prediction model, polynomial degree is $m = 1$ and number of samples used in fitting/training is $n = 1220$.

In this paper, the receiver starts prediction calculations upon the receipt of the first codeword which code rate is chosen to be $8/16$ for simulation purposes. Since each fade represents 1024 bits, the receiver will estimate 16 channel gain values. This is the smallest number of samples used to fit a polynomial to predict a future channel gain. As more samples arrive at the receiver, each new prediction is modeled using more samples. For the purpose of evaluating prediction models the codewords received until first codeword encoded with predicted rate arrives at the receiver are considered as pilots and not used for analysis.

4) Training Samples Selection

The number of channel gain samples used in the prediction models is determined using a greedy optimization approach by solving the following minimization problem:

$$\min_{j} MSE = \frac{1}{N}\sum_{i=1}^{N}(\hat{\rho}_i - \tilde{\rho}_i^{(j)})^2,\ j = 1, 2, ..., l \in \mathbb{N}, \tag{27}$$

where $\hat{\rho}_i$ are estimated fading channel gain values at the receiver, $\tilde{\rho}_i^{(j)}$ are predicted channel gain values solving (26), N is the number of data points and j represents the index of vector with length l containing number of data points in

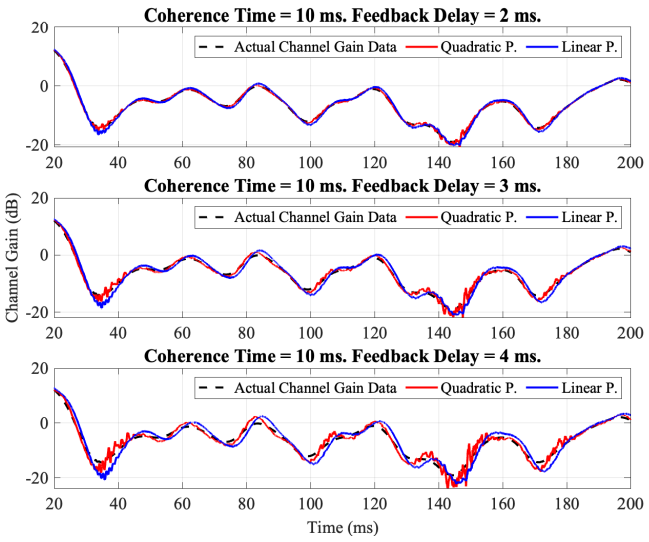

FIGURE 10. **Comparison of channel gain values for quadratic and linear prediction with respect to the actual fading channel gain values when coherence time is $10\ ms$ and feedback delay ranges from $2\ ms$ to $4\ ms$.**

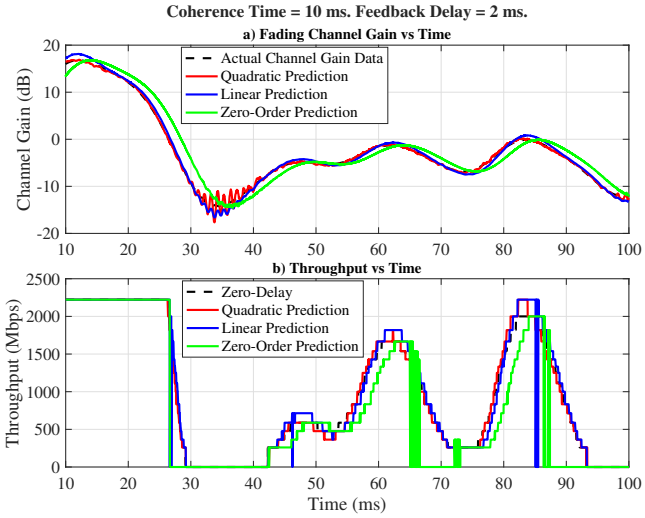

FIGURE 11. **a) Actual and predicted channel gain values vs. time. b) Throughput vs. time obtained using zero-delay, zero-order, linear and quadratic prediction models for fading channel conditions in a). Turbulence coherence time is $10\ ms$, feedback delay is $2\ ms$ and baud rate is $2.5\ Gbps$.**

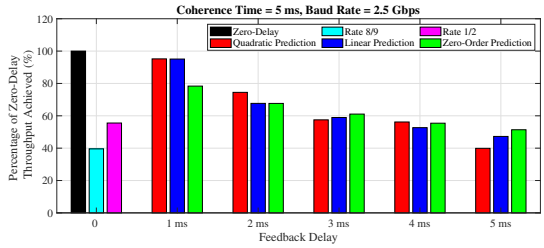

FIGURE 12. **Percentage of zero-delay throughput achieved using prediction models as a function of feedback delay when coherence time is $5\ ms$ and feedback delay ranges from $1\ ms$ to $5\ ms$. Quadratic prediction model gives the best performance for shorter feedback delay times ($1\ ms$ and $2\ ms$). Zero-Order prediction model gives the best performance for longer feedback delay times. Simulation is performed for $80\ ms$.**

ms starting from $0.5\ ms$ up to coherence time of optical channel in increments of $0.5\ ms$. The number of data points N used in (27) corresponds to number of predicted $\tilde{\rho}_i^{(j)}$ in (26) over duration of $200\ ms$ for every j. For example, for a channel coherence time of $5\ ms$, j would range from 1 to 10, where index $j = 1$ represents $0.5\ ms$ worth of data points and index $j = l = 10$ represents $5\ ms$ worth of data. The solution of (27) for the linear prediction model suggests that $0.5\ ms$ worth of data gives the best fitting performance for both coherence times considered.

5) Quadratic Prediction

The quadratic prediction model uses $m = 2$ in (25), using past and current estimated CSI in a quadratic model to predict future CSI for LDPC code rate selection. The number of channel gain samples used in quadratic prediction is equal to $1\ ms$ and $2\ ms$ for optical channels with coherence times of $5\ ms$ and $10\ ms$ respectively. These values are obtained by solving (27). For all prediction models, we observed that adding a small margin of $0.25\ dB$ to the original crossing points determined in Table 2 when selecting LDPC code rate at the receiver improved our FER performance.

Fig. 10 compares channel gain data obtained using linear and quadratic prediction models when feedback delay increases from $2\ ms$ to $4\ ms$ with actual channel gain data over the time interval of $10\ ms$ to $100\ ms$. As feedback delays increases, the prediction becomes worse. Quadratic prediction becomes noisy when the channel is very bad, mainly due to noisy fading channel gain estimation in this area.

Fig. 11 a) shows actual and predicted channel gain values for zero-order, linear and quadratic prediction when turbulence coherence time is $10\ ms$ and feedback channel delay is $2\ ms$. Fig. 11 b) shows throughput as a function of time obtained using prediction models in Fig. 11 a). Linear and quadratic prediction models give similar performance as baseline zero-delay model, while zero-order prediction show loss in throughput compared to other models.

C. Computational Complexity

Polynomial regression fits a polynomial function of degree m to a data set. For linear $(m = 1)$ and quadratic $(m = 2)$ prediction models, the computational complexity depends on the number of data points n and polynomial degree m. The computational complexity of the prediction models involves the following steps:

- Complexity $\mathcal{O}(nm)$: Input data are transformed into polynomial features. For linear prediction $(m = 1)$ this includes t_i term, and for quadratic prediction $(m = 2)$ this includes t_i and t_i^2 terms, where $i = 1, 2, ..., n$. We are not counting column of all ones in matrix $\boldsymbol{A}$.

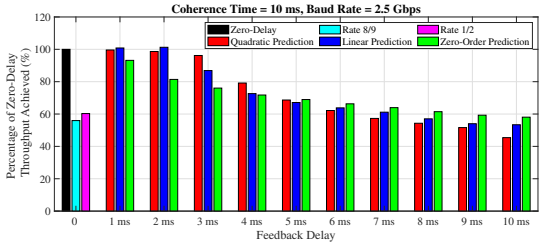

FIGURE 13. **Percentage of zero-delay throughput achieved using prediction models as a function of feedback delay when coherence time is $10\ ms$ and feedback delay ranges from $1\ ms$ to $10\ ms$. Quadratic prediction model gives the best performance for shorter feedback delay times ($1\ ms$ to $5\ ms$). Zero-Order prediction model gives the best performance for longer feedback delay times. Simulation is performed for $160\ ms$.**

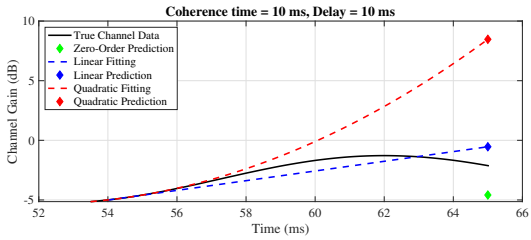

FIGURE 14. **Comparison of zero-order, linear and quadratic predictions of channel gain value at time instance of $65\ ms$ for feedback delay of $10\ ms$ and coherence time of $10\ ms$. The amount of data used for linear and quadratic predictions is equal to $0.5\ ms$ and $2\ ms$, respectively.**

- Complexity $\mathcal{O}(nm^2 + nm + m^3)$: The least squares solution involves solving:

$$\boldsymbol{x} = (\boldsymbol{A}^T\boldsymbol{A})^{-1}\boldsymbol{A}^T\ \hat{\boldsymbol{\rho}}.$$

  - Compute $\boldsymbol{A}^T\boldsymbol{A}$ (matrix multiplication): $\mathcal{O}(nm^2)$
  - Compute the inverse of $\boldsymbol{A}^T\boldsymbol{A}$: $\mathcal{O}(m^3)$
  - Compute $\boldsymbol{A}^T\ \hat{\boldsymbol{\rho}}$: $\mathcal{O}(nm)$

Total complexity for both prediction models is $\mathcal{O}(nm^2 + 2nm + m^3)$. For the linear prediction model, $n = 1220$ for both coherence times of $5\ ms$ and $10\ ms$. For the quadratic prediction model, the number of samples n is 2440 and 4880 for fading channels with coherence times 5 and $10\ ms$, respectively.

D. Prediction Models Performance

Fig. 12 shows the percentage of zero-delay throughput achieved using each prediction model and single rates $8/9$ and $1/2$ as a function of feedback delay when coherence time is $5\ ms$. The feedback delay ranges from $1\ ms$ to $5\ ms$ and data is collected for $160\ ms$. The quadratic prediction model gives the best performance for shorter delay times achieving 95.2% and 74.5% of zero-delay throughput for feedback delays of $1\ ms$ and $2\ ms$, respectively. For feedback delays $3-5\ ms$, zero-order prediction outperforms linear and quadratic models. Throughput achieved using single rates $8/9$ and $1/2$ are 39.6% and 55.5%, respectively.

Fig. 13 depicts the percentage of zero-delay throughput achieved using each prediction models and single rates ($8/9$ and $1/2$) as a function of feedback delay when coherence time is $10\ ms$. The linear prediction model gives the best performance for $1\ ms$ and $2\ ms$ feedback delays achieving 100.8% and 101.2% of zero-delay throughput, respectively. Note that 101.3% is due to the linear prediction model occasionally overestimating channel gain values at the peaks where the values change direction from increasing to decreasing. At these peaks, the model sometimes successfully selects a higher code rate compared to zero-delay model. Since we are considering crossing points where the LDPC code achieves FER below 10^{-6}, the selected code rate might still have a high chance of success, which happened in the simulation for 1 and $2\ ms$ feedback delay.

Quadratic model outperforms other prediction models for $3-5\ ms$ feedback delays achieving from 68.7% to 95.2% of zero-delay throughput. Zero-order prediction achieves the highest throughput for longer feedback delays $6-10\ ms$.

Quadratic prediction is worse than linear and zero-order predictions for longer feedback delays because it overestimates channel gain values near peaks in data. For example, Fig. 14 compares prediction models when predicting channel gain value at time instance of $65\ ms$ for feedback delay of $10\ ms$ and coherence time of $10\ ms$. Quadratic prediction overestimates channel gain values by $10\ dB$, which results in selecting rate $8/9$ that the true channel condition cannot support as evident in Fig. 8 b). Zero-order prediction is the only model that underestimates channel gain values at peaks and selects a lower rate than what channel can support, which results in successful decoding but smaller throughput than baseline zero-delay throughput.

The single rate choice of using only rate $1/2$ seems to be a preferable choice for feedback delays longer than $8\ ms$. However, this is true only if the atmospheric turbulence is not too strong to severely degrade the channel. In such cases, long outages are possible as seen approximately between $30\ ms$ and $80\ ms$ in Fig. 8 b).

VI. Conclusions

For an FSO fading channel when CSI is known with no delay, the throughput is maximized by selecting the rate accordingly. This paper presents three prediction models to mitigate FSO fading when feedback delay is not zero.

The simulation results indicate that the quadratic prediction model is the overall best choice for round-trip feedback delays shorter than half of the fading channel coherence time τ_0. For $\tau_0 = 5\ ms$, quadratic model achieves from 95.2% to 74.6% of the zero-delay throughput as round-trip feedback delay increases from $1\ ms$ to $\lfloor \tau_0/2 \rfloor\ ms$. For a fading optical channel with a coherence time of $10\ ms$ simulation results show that using only a single LDPC code rate $8/9$ or $1/2$ results in up to 55.9% or 60.3% of zero-delay throughput, respectively. In comparison, for the same channel for shorter feedback delays ($1\ ms$ to $5\ ms$) quadratic model achieves $(99.6-68.7)\%$ of zero-delay throughput. For

feedback delays 6 ms and 7 ms zero-order prediction model achieves $(66.3 - 64.0)\%$ of the zero-delay throughput.

While quadratic model works very well for shorter feedback delays, prediction for longer feedback delays can be improved. Quadratic polynomial fitting fails to predict the change in fading channel gain at the peaks where the channel gain values change direction from increasing to decreasing, and this leads to poor prediction for longer feedback delays. Our future work will aim to mitigate this problem through various approaches, including machine learning techniques such as neural network regression.

REFERENCES

[1] M. Leba, S. Riurean, and A. Lonica, "Lifi — the path to a new way of communication," in *2017 12th Iberian Conference on Information Systems and Technologies (CISTI)*, 2017, pp. 1–6.

[2] M. A. Khalighi and M. Uysal, "Survey on free space optical communication: A communication theory perspective," *IEEE Communications Surveys & Tutorials*, vol. 16, no. 4, pp. 2231–2258, 2014.

[3] H. T. T. Pham, N. T. Dang, L. T. Vu, and H. T. Bui, "A survey of performance improvement methods for free-space optical communication systems," in *2014 International Conference on Advanced Technologies for Communications (ATC 2014)*, 2014, pp. 770–775.

[4] M. Uysal and H. Nouri, "Optical wireless communications — an emerging technology," in *2014 16th International Conference on Transparent Optical Networks (ICTON)*, 2014, pp. 1–7.

[5] B. Bag, A. Das, I. S. Ansari, A. Prokeš, C. Bose, and A. Chandra, "Performance analysis of hybrid FSO systems using FSO/RF-FSO link adaptation," *IEEE Photonics Journal*, vol. 10, no. 3, pp. 1–17, 2018.

[6] M. N. Khan, S. O. Gilani, M. Jamil, A. Rafay, Q. Awais, B. A. Khawaja, M. Uzair, and A. W. Malik, "Maximizing throughput of hybrid FSO-RF communication system: An algorithm," *IEEE Access*, vol. 6, pp. 30 039–30 048, 2018.

[7] M. M. Abadi, Z. Ghassemlooy, S. Zvanovec, M. R. Bhatnagar, and Y. Wu, "Hard switching in hybrid FSO/RF link: Investigating data rate and link availability," in *2017 IEEE International Conference on Communications Workshops (ICC Workshops)*, 2017, pp. 463–468.

[8] J. Nguyen, E. M. Liang, L. Wang, R. D. Wesel, T. Drullinger, and T. Chauvin, "Comparison of integrated and independent RF/FSO transceivers on a fading optical channel," in *2020 54th Asilomar Conference on Signals, Systems, and Computers*, 2020, pp. 699–701.

[9] A. Eslami, S. Vangala, and H. Pishro-Nik, "Hybrid channel codes for efficient FSO/RF communication systems," *IEEE Transactions on Communications*, vol. 58, no. 10, pp. 2926–2938, 2010.

[10] A. García-Zambrana, C. Castillo-Vázquez, and B. Castillo-Vázquez, "Rate-adaptive FSO links over atmospheric turbulence channels by jointly using repetition coding and silence periods," *Opt. Express*, vol. 18, no. 24, pp. 25 422–25 440, Nov 2010. [Online]. Available: https://opg.optica.org/oe/abstract.cfm?URI=oe-18-24-25422

[11] M. Czaputa, T. Javornik, E. Leitgeb, G. Kandus, and Z. Ghassemlooy, "Investigation of punctured LDPC codes and time-diversity on free-space optical links," in *Proceedings of the 11th International Conference on Telecommunications*, 2011, pp. 359–362.

[12] I. B. Djordjevic, "Adaptive modulation and coding for free-space optical channels," *Journal of Optical Communications and Networking*, vol. 2, no. 5, pp. 221–229, 2010.

[13] J. A. Anguita, M. A. Neifeld, B. Hildner, and B. Vasic, "Rateless coding on experimental temporally correlated FSO channels," *Journal of Lightwave Technology*, vol. 28, no. 7, pp. 990–1002, 2010.

[14] L. Liu, M. Safari, and S. Hranilovic, "Rate-adaptive FSO communication via rate-compatible punctured LDPC codes," in *2013 IEEE International Conference on Communications (ICC)*, 2013, pp. 3948–3952.

[15] T. Mizuochi, "Recent progress in forward error correction and its interplay with transmission impairments," *IEEE Journal of Selected Topics in Quantum Electronics*, vol. 12, no. 4, pp. 544–554, 2006.

[16] B. Vasic and O. Milenkovic, "Combinatorial constructions of low-density parity-check codes for iterative decoding," *IEEE Transactions on Information Theory*, vol. 50, no. 6, pp. 1156–1176, 2004.

[17] B. Vasic and I. B. Djordjevic, "Iteratively decodable block codes for long haul optical transmission systems," *Journal of Optical Communications*, vol. 23, no. 5, pp. 182–186, 2002. [Online]. Available: https://doi.org/10.1515/JOC.2002.23.5.182

[18] European Telecommunications Standards Institute (ETSI), "Digital Video Broadcasting (DVB); Second generation framing structure, channel coding and modulation systems for broadcasting, interactive services, news gathering and other broadband satellite applications (DVB-S2)." European Telecommunications Standards Institute (ETSI), Tech. Rep. EN 302 307 V1.2.1, 2009.

[19] Space Development Agency, "Optical Communications Terminal (OCT) standard version 3.1.0." Space Development Agency, Tech. Rep., 2023.

[20] T.-Y. Chen, K. Vakilinia, D. Divsalar, and R. D. Wesel, "Protograph-based raptor-like LDPC codes," *IEEE Transactions on Communications*, vol. 63, no. 5, pp. 1522–1532, 2015.

[21] S. Galijasevic, J. Luo, D. Divsalar, and R. Wesel, "Effect of feedback delay on adaptive ldpc coding in a fading free-space optical channel," in *ICC 2024 - IEEE International Conference on Communications*, 2024, pp. 2420–2426.

[22] M. W. Wright, M. Srinivasan, and K. Wilson, "Improved Optical Communications Performance Using Adaptive Optics with an Avalanche Photodiode Detector," *Interplanetary Network Progress Report*, vol. 42-161, pp. 1–13, May 2005.

[23] Z. Kolka, V. Biolková, and D. Biolek, "Channel model for monte-carlo simulation of data transmission on terrestrial FSO paths," in *International Conference on Emerging Trends in Engineering and Technology*, 2014. [Online]. Available: https://api.semanticscholar.org/CorpusID:53313155

[24] Y. Polyanskiy, H. V. Poor, and S. Verdu, "Channel coding rate in the finite blocklength regime," *IEEE Transactions on Information Theory*, vol. 56, no. 5, pp. 2307–2359, 2010.

[25] "LDPC HRC and IRC proto-matrices for FSO Channel." [Online]. Available: http://www.seas.ucla.edu/csl/publications/published-codes-and-design-tools

[26] T. Tian, C. Jones, J. Villasenor, and R. Wesel, "Selective avoidance of cycles in irregular LDPC code construction," *IEEE Transactions on Communications*, vol. 52, no. 8, pp. 1242–1247, 2004.

[27] Consultative Committee for Space Data Systems (CCSDS), "Non-Coherent Optical Communications Coding and Synchronization," CCSDS, Tech. Rep. CCSDS 142.0-P-1.1, November 2023, draft Recommended Standard (Pink Sheets).

[28] S. Boyd and L. Vandenberghe, *Convex Optimization*. Cambridge University Press, 2004, ch. 6.5.3.

SEMIRA GALIJASEVIC (Student Member, IEEE) received her BS degree (Summa Cum Laude) and MS degree in Electrical Engineering from the University of California at Los Angeles (UCLA) in 2021 and 2023, respectively. She is currently pursuing a Ph.D. degree in Electrical Engineering at UCLA with the Communications Systems Laboratory. Her research interests include information theory, channel coding theory, LDPC codes, adaptive coding in fading optical channels, coding for storage, and optimal modulation design.

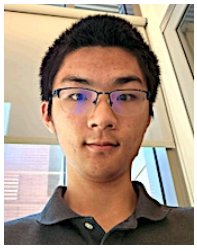

JINGCHAO LUO (Student Member, IEEE) is currently pursuing his BS degree in Electrical Engineering at the University of California Los Angeles (UCLA 2026). He is currently an undergraduate researcher at the UCLA Communication Systems Laboratory under Professor Richard Wesel. His interests include channel coding theory, wireless communications, digital signal processing, and FPGA development.

DARIUSH DIVSALAR (Life Fellow, IEEE) received the Ph.D. degree in electrical engineering from UCLA, in 1978. Since then, he has been with the Jet Propulsion Laboratory (JPL), California Institute of Technology (Caltech), Pasadena, where he is a Fellow. At JPL, he has been involved with developing state-of-the-art technology for advanced deep-space communications systems and future NASA space exploration. Since 1986, he has taught graduate courses in communications and coding at UCLA and Caltech. He has published more than 295 papers, coauthored a book, contributed to three other books, and holds 30 U.S. patents. Dr. Divsalar was a co-recipient of the 1986 paper award of the IEEE Transactions on Vehicular Technology. He was also a co-recipient of the joint paper award of the IEEE Information Theory and IEEE Communication Theory societies in 2008. The IEEE Communication Society has selected one of his papers for inclusion in a book entitled The Best of the Best: Fifty Years of Communications and Networking Research. He served as an Editor for the IEEE Transactions on communications from 1989 to 1996. A fellow of IEEE since 1997. He has received over 50 NASA Tech Brief awards, a NASA Exceptional Engineering Achievement Medal in 1996, IEEE Alexander Graham Bell Medal in 2014, an Ellis Island Medal of Honor in 2023, and a NASA Distinguished Public Service Medal in 2023. He has been elected to the National Academy of Engineering in 2024.

RICHARD WESEL (Fellow, IEEE) received the B.S. and M.S. degrees in electrical engineering from the Massachusetts Institute of Technology in 1989 and the Ph.D. degree in electrical engineering from Stanford University in 1996. He is currently a Professor with the Electrical and Computer Engineering Department, Henry Samueli School of Engineering and Applied Science, UCLA, where he is also the Associate Dean of Academic and Student Affairs. His research interests include communication theory with a particular interests in short-blocklength communication with and without feedback, list decoding, low-density parity-check codes, and optimal modulation design. Dr. Wesel is a Fellow of the IEEE and has received the National Science Foundation CAREER Award, the Okawa Foundation Award for Research in Information Theory and Telecommunications, and the Excellence in Teaching Award from the Samueli School of Engineering. He has served as an Associate Editor for Coding and Coded Modulation and IEEE Transactions on Communications and as an Associate Editor for Coding and Decoding and IEEE Transactions on Information Theory.